Nuclear Engineering and Design 265 (2013) 1036–1044

Contents lists available at ScienceDirect

Nuclear Engineering and Design

journal homepage: www.elsevier.com/locate/nucengdes

Heat transfer in CO_2 at supercritical pressures in an eccentric annular channel

Yoon-Yeong Bae*

Korea Atomic Energy Research Institute, 989-111 Daedeokdaero, Yuseong, Daejeon 305-353, Republic of Korea

HIGHLIGHTS

- Heat transfer under supercritical pressure in an eccentric annular channel pressure was studied.
- The studied geometry was an eccentric annular channel with an eccentricity of 0.33.
- The effect of spacer as a turbulence generator was investigated.
- The effects of the mass flux, heat flux, and pressure were investigated.
- The obtained data were evaluated against the correlation.

ARTICLE INFO

Article history:
Received 23 August 2013
Received in revised form 1 October 2013
Accepted 8 October 2013

ABSTRACT

An experimental investigation of a supercritical heat transfer in an eccentric annular channel was performed using a supercritical heat transfer test facility, SPHINX, at the Korea Atomic Energy Research Institute (KAERI). The eccentric channel was built by placing a 9.5 mm outer diameter heater rod in a 12.5 mm inner diameter tube with an eccentricity of 0.33. The narrowest gap was 1 mm, and the widest gap was 2 mm. The rod was heated indirectly by an imbedded Nickel Chrome heating wire made of NCHW1. Three simple spacers were installed to see their effect, if any, on the heat transfer. The mass fluxes were 400 and 1200 kg/m^2 s, and the heat flux was varied between 30 and 150 kW/m^2 such that the pseudo-critical point was located within the test section as long as possible. When this was not the case, several tests with stepwise increased inlet temperatures were performed so that at least one of them included the pseudo-critical point. The tests were performed at two different pressures of 7.75 and 8.12 MPa to check the pressure effect. The influence of the gap size was clearly seen with the eccentric channel, if not significant. The wall temperatures along the narrowest gap were higher than those along the widest gap as expected, while it was reversed at the end part of the test section. The test results for the eccentric channel were not much different from those for the concentric channel of a similar gap size. As we have seen from the plain tube test, the diameter effect on the heat transfer was also not significant in this test. On the contrary, the effect of the spacer as a turbulence generator was noticeable, particularly at the thermocouples, which were 10 mm downstream from the trailing edge of the first spacer.

1. Introduction

Heat transfer at a supercritical pressure has been studied enthusiastically since the introduction of fossil-fuel fired power plants between the 1950s and early 1970s. The major concern at that time was the integrity of the boiler tube. After saturation of the research, interest in supercritical heat transfer had diminished to almost nothing until a revisit of the subject was initiated by a reinstated interest in a Super-Critical (pressure) Water-cooled Reactor (SCWR) and heat exchangers using supercritical CO_2 as a medium, to name a few.

The heat transfer at a super-critical pressure is totally different from that at subcritical pressures owing to the substantial variations of the physical properties of fluids at around the pseudo-critical temperature,[1] as shown in Fig. 1. The convective heat transfer correlations developed based on the test data obtained at

* Corresponding author at: Reactor System Technology Development Department, Korea Atomic Energy Research Institute, 989-111 Daedeokdaero, Yuseong, Daejeon 305-353, Republic of Korea. Tel.: +82 42 868 8130; fax: +82 42 868 8767.
E-mail address: yybae@kaeri.re.kr

[1] Over the critical pressure, a substantial change in the physical properties still occurs around a particular temperature, which is called the pseudocritical temperature as an analogy with the critical temperature, which corresponds to the critical pressure.

0029-5493/$ – see front matter © 2013 Elsevier B.V. All rights reserved.
http://dx.doi.org/10.1016/j.nucengdes.2013.10.005

Nomenclature

Bu	buoyancy parameter, $Bu = \overline{Gr}_b/Re_b^{2.7}$
$\overline{C_p}$	average specific heat, $\int_{T_b}^{T_w} C_p dT/(T_w - T_b)$
D	diameter (m)
D_h	hydraulic diameter (m)
e	eccentricity, $e = l/(R_o - R_i)$
G	mass flux (kg/m^2 s)
$\overline{Gr}_b$	Grahhof number, $\rho_b(\rho_b - \bar{\rho})gD^3/\mu_b^2$
g	gravitational acceleration (m/s^2)
l	distance between centerlines of rod and tube (m)
Nu	Nusselt number, hD/k
p	pressure (Pa)
$\overline{Pr}$	Prandtl number based on $\overline{C_p}$
q	heat flux (kW/m^2)
R	radius (m)
Re	Reynolds number, GD/μ
T	temperature (K)

Greek Letters

ρ	density (kg/m^3)
$\bar{\rho}$	average density, $\int_{T_b}^{T_w} \rho dT/(T_w - T_b)$
μ	dynamic viscosity (Pa s)

Subscripts

b	mass averaged value
i	inner
in	at the inlet
o	outer
pc	at pseudocritical temperature
w	at the wall

subcritical pressures are no longer valid for applications at supercritical pressures since the non-dimensional parameters based on the bulk temperature or the averaged temperature are not sufficient to interpret the flow and thermal fields at supercritical pressures. In this regime the properties at a wall temperature begin to play an important role and should be reflected in a heat transfer correlation. A change in the temperature and a resulting change in the physical properties primarily occur near a wall. When the location of the pseudocritical temperature appears at a near-wall region, the variation of the physical properties will be substantial around this location, and the heat transfer rate must be a function of these varying properties. Jackson (2002) proposed a correlation after analyzing extensive experimental data from various sources, but did not address a deterioration regime. Based on their test data with Freon, Komita et al. (2003) modified a correlation suggested by Watts and Chou (1982). Bae and Kim (2008) recently proposed a supercritical heat transfer correlation based on experiments with CO_2 in an attempt to cover both the normal and deteriorated regimes by a group of correlations.

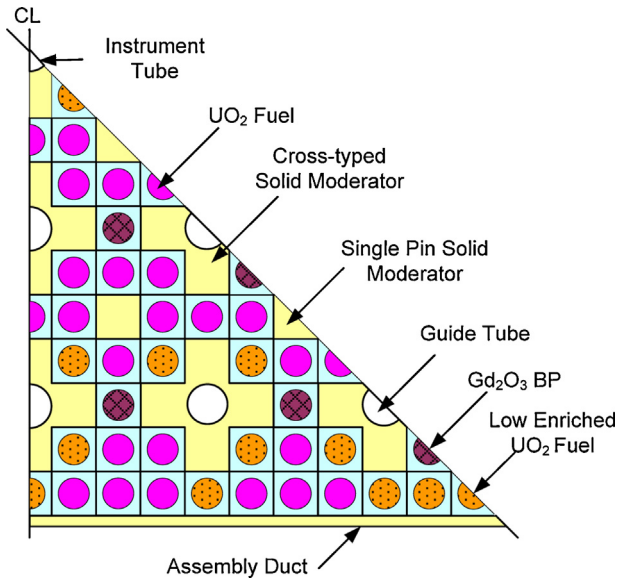

Fig. 2. Cross-sectional view of fuel assembly model suggested by KAERI.

The subchannels in a fuel assembly under the SCWR concept proposed by KAERI are narrower than those in a conventional PWR or BWR owing to a neutronics consideration (Bae et al., 2007). Moreover, the subchannels are different from each other in size and shape, as shown in Fig. 2.

Waata et al. (2005), using a subchannel code STAFAS and Monet Carlo code MCNP, showed that the cladding surface temperature of the fuel rod adjacent to the corner was systematically higher than others. The difference can be attributed to a poor mixing and low flow rate. Sharabi et al. (2008) used the commercial Computational Fluid Dynamics (CFD) code Fluent for the calculation of the problems, which Waata et al. (2005) studied. The calculations

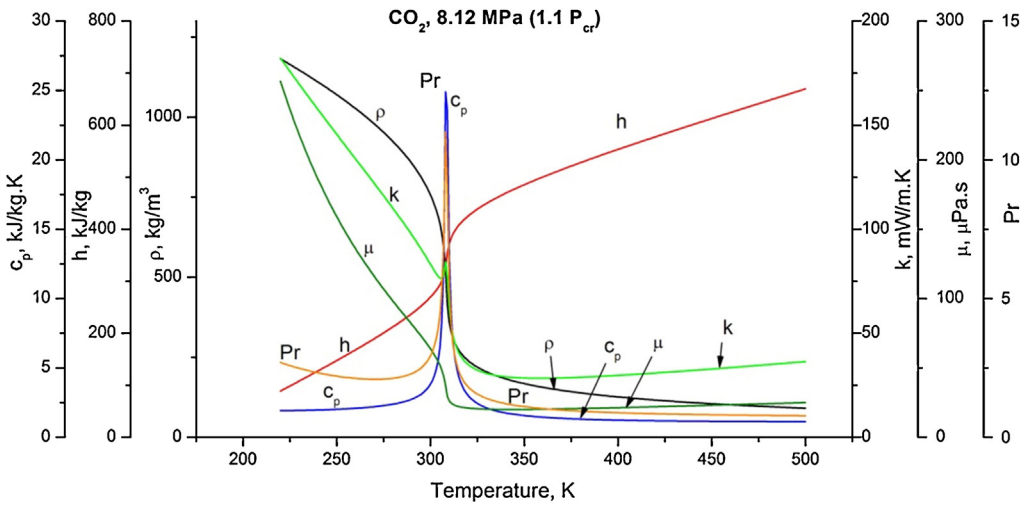

Fig. 1. Property variation of CO_2 at a pressure of 110% of the critical pressure.

performed in their work showed that the CFD code predicted details in the mass flux distribution among subchannels in a different way with respect to the predictions by one-dimensional subchannel approaches.

Nouri et al. (1993) studied experimentally a flow of Newtonian fluids in eccentric annuli with inner and outer diameter of the channel of 20.1 mm and 40.3 mm, respectively. The eccentricities were 0, 0.5 and 1.0 Nouri et al. showed that the turbulence intensity and shear stress were smallest in the narrowest gap, and that the variation of the mean velocity was considerable.

Okumura et al. (2006) simulated a fully developed turbulent flow in an eccentric annular channel, where the diameter ratio was 0.5 and the eccentricity was 0.5, using the Direct Numerical Simulation (DNS), and confirmed an occurrence of laminarization in a narrowest channel. In their calculation, the Reynolds number based on a bulk flow was 12,100. As is evident from the references cited above, the low mass flux and accompanying laminarization (or at least weak turbulence) in the narrowest gap may be partly responsible for the higher temperature in the narrowest gap.

Rapley and Gosman (1986) performed a numerical simulation of a fully developed axial turbulent flow in a rod bundles. Rapley and Gosman reported that the wall shear stress in a narrower gap was lower than that in a wider gap. The numerical simulation with a secondary flow confirmed the circumferentially inhomogeneous shear stress distribution along a fuel pin surface. When the P/D increases to 1.2, they reported that the shear stress showed almost an even distribution along the fuel pin surface. This may imply that the narrower gap is more susceptible to laminarization and a possible sudden jump of the wall temperature or corresponding heat transfer deterioration.

Considering this non-uniformity in the temperature distribution in a fuel assembly, an accurate estimation of the cladding temperature is very important for the proper design of the fuel assembly and the performance of the reactor core. The heat transfer correlations proposed thus far are still subject to improvement since they show non-negligible differences in the vicinity of the pseudocritical temperature, where an undesirable heat transfer deterioration may occur. With this uncertainty in the heat transfer correlation, a numerical simulation has an apparent limitation in providing an accurate estimation of the fuel cladding surface temperature and the bulk temperature of the coolant in the subchannel.

To the author's best knowledge, there has never been an attempt to measure the temperatures in a narrow eccentric annular channel at a supercritical pressure, which is no doubt required to study the flow and thermal phenomena in the subchannel of the fuel assembly and to eventually optimally design the SCWR. In this respect, an experimental study on the thermal behavior in an eccentric annular channel was initiated. The experiment was supposed to provide preliminary information on the extent of the temperature difference between different channels rather than giving exact design information. In this study, we intended to investigate the gap size effect on the surface temperature distribution. In addition to the channel size effect, the effect of a spacer was also investigated by installing three simple spacers along the annulus channel. It was expected that the test undertaken by this work will provide valuable, if qualitative, information for the design of the SCWR. A test representing the actual design parameters such as the pressure, mass flux, and heat flux, as well as the dimensions of the fuel assembly, remains for a further study.

2. Experiment

2.1. Experimental facility

Since the critical conditions of water are 22.12 MPa and 374.14 °C, and a heat transfer test under such conditions requires a high heating power and cost, CO_2 has been widely used as a surrogate fluid, which has a much milder critical condition (7.38 MPa, 31.05 °C) than water. In our test, we chose CO_2 as a medium to take advantage of its low critical condition and low experimental cost. Fig. 3 shows a schematic diagram of the test facility. The design pressure and temperature of the main loop are 12.0 MPa and 80 °C, respectively.

The test loop is initially charged with CO_2 by an air-driven reciprocating compressor. The charged CO_2 is pumped by two gear pumps installed in parallel to the bottom of the test section through the electric heater, which heats up the fluid to the pre-set fluid temperature at the test section inlet. The CO_2 leaving the test section enters the heat exchanger and cools down to the pre-set temperature. The heat exchanger is cooled by chilled water, and the chilled water temperature is controlled by a cooler. A gear-type pump is adopted to minimize the inevitable flow fluctuation. The accumulator filled with gaseous nitrogen, which is located at the discharge of the pumps, also reduces any fluctuation in the flow. The pre-heater and power supply unit control the inlet and outlet temperatures of the fluid, respectively. The test section is heated by an indirect electric heating to provide a uniform heat flux to the test section surface. The mass flow rate is regulated by adjusting the bypass valve and/or pump speed. A Corioli type flow meter, manual flow control and isolation valves, pressure transmitters, and thermocouples are installed in the test facility. The inner diameter of the main loop is about 20 mm. The main loop is insulated to minimize any heat loss to the atmosphere.

2.2. Test sections

The annular channel is constructed between a 12.5 mm inner diameter tube and a 9.5 mm outer diameter heater rod eccentrically placed in it. The narrowest gap is 1 mm and the widest gap is 2 mm. The eccentricity defined as $e = l/(R_o - R_i)$ is 0.33.

The tube is surrounded by an outer housing. A stagnant CO_2 occupies the space between the enclosure tube and the outer housing. The CO_2 at the pre-determined temperature and pressure is heated as it flows upward through the annular channel. The flange-to-flange length is 2631 mm and the heated length is 1800 mm. The heater rod is a tube-type sheath made of NCF600 filled with Boron Nitride (BN). The heater rod is heated indirectly by a Nickel-Chrome heating coil made of NCHW1 imbedded in the Boron Nitride core, which acts as an insulator between the sheath and the heating coil. Sixteen (16) thermocouples are inserted into grooves machined on the outer surface of the sheath. The locations of the thermocouples are as shown in Fig. 4(a). The tips (3 mm) are TIG welded and 100 mm from the tips is welded by Ag brazing as shown in Fig. 4(b). At the upper and lower ends, mixing plenums are provided for the supply of thermally homogeneous CO_2 into the annulus channel. Three spacers 30 mm in length are installed upstream of the third, fifth, and seventh rows of the thermocouples with distances 10, 50, and 100 mm each from the trailing end of the spacers. The distances from the trailing edge of the spacers are approximately 3, 17, and $33D_h$, respectively. The configuration of the spacer is shown in Fig. 4(c). The thickness of the spacer is 0.4 mm. The centerline of the spacer was aligned with the centerline of the heater rod and the position was secured by a wire of 1 mm in diameter inserted along the widest gap of the channel, and two wires of 0.5 mm diameter inserted in a similar fashion at the 90° and 270° positions. The hydraulic diameter based on the wetted perimeter of the channel is 3.0 mm.

2.3. Experimental procedure

The tests were conducted by changing the mass flux and heat flux at given pressures. To investigate the effects of pressure on the

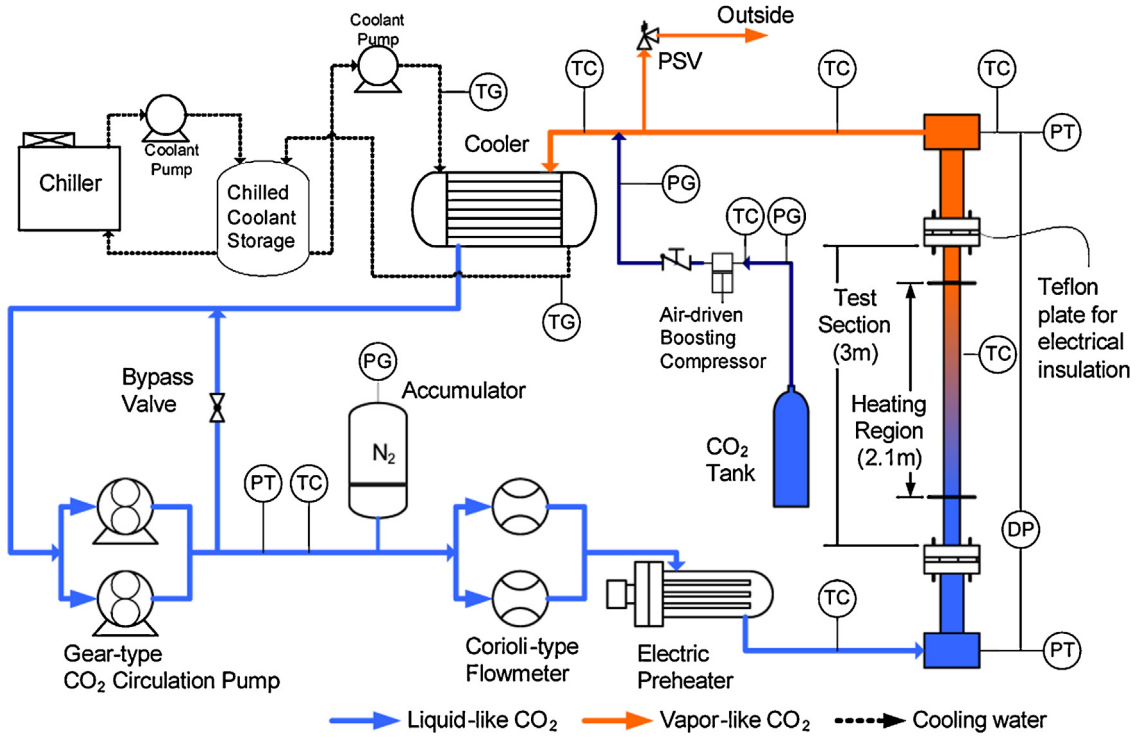

Fig. 3. Schematic of the supercritical CO_2 heat transfer test facility, SPHINX.

heat transfer, the experiments were performed at two different pressures: 105 and 110% of the critical pressure. The bulk temperature at the test section outlet is restricted to below 100 °C for safety reasons. For each test, the heat flux was determined for a given mass flux and pressure so that the fluid temperature passes the pseudocritical point well ahead of the exit of the test section. When it was not possible, the enthalpy range was divided into several smaller ranges, and a separate test was performed for each range. This constraint was imposed to guarantee the occurrence of heat transfer deteriorations in the test section. Table 1 shows a summary of the test conditions. The range of the Reynolds number was 1.17×10^4–1.37×10^5, which was carefully chosen to cover the operating range of the SCWR concept proposed by KAERI. Obviously, the fluid is turbulent unless a strong laminarization locally appears owing to a sudden decrease in density. Please note that for the calculation of Reynolds number, an equivalent hydraulic diameter based on a wetted perimeter instead of a heated perimeter was used.

2.4. Data acquisition and uncertainty analysis

A PC-based DAS (data acquisition system) was used to collect the test data. The assembly of a VXI-based multiplexer and multimeter scanned and digitized the process variables from the loop, and then transferred them to the PC over an IEEE1394 bus. This equipment can scan 64 channels at a rate of 300 Hz. The number of process variables in the loop was 52, and the experiments were implemented under a steady state. The accuracies and ranges of the measuring devices are shown in Table 2. Near a pseudocritical temperature, the wall temperature approached the bulk fluid temperature to as close as a few degrees Celsius. Such a small temperature difference was comparable with the standard accuracy of a K-type T/C, and it might have caused a considerable error in an estimated heat transfer coefficient (HTC). Thus, a specific in situ calibration was performed to clarify the error bound of the test results. The T/Cs were calibrated, both at cooled and heated conditions, using a thermometer, and the maximum error was less than 2.0%. The differences between the readings at DAS and the thermometer were checked under cooled and heated conditions (about 54 kW/m^2). The maximum relative error between the DAS and thermometer was 1.49%. The total uncertainty of the measured data is 2.49% [square root of (thermocouple accuracy)^2 + (DAS accuracy)^2], neglecting the uncertainty in the electric heating power.

The physical properties of carbon dioxide were calculated from the NIST package (Lemmon et al., 2010).

3. Results and discussion

The required enthalpy range for a particular case cannot possibly be covered by a single test owing to a limitation of the power supply. In this case, the enthalpy range was divided into several ranges and a series of experiments were performed with progressively increased inlet temperatures so that the prescribed enthalpy range was covered with the pseudocritical temperature within its range. The leading part of the succeeding plot does not exactly overlap onto the trailing part of the preceding plot, since there must

Table 1
Test conditions.

Conditions	Value
Inlet pressure (MPa)	7.75, 8.12 (1.05, 1.10 P_{cr})
Inlet temperature (°C)	5–40
Mass flux (kg/m^2 s)	400, 1200
Heat flux (kW/m^2)	30–150
Reynolds number	1.17×10^4 to 1.37×10^5

Table 2
Accuracies and ranges of the measuring instruments (Vendor supplied).

Measuring instrument	Range	Accuracy
K-type thermocouple	0–1260 °C	±0.75% or ±2.2 °C
Mass flow meter	0–680 kg/h	±0.15%

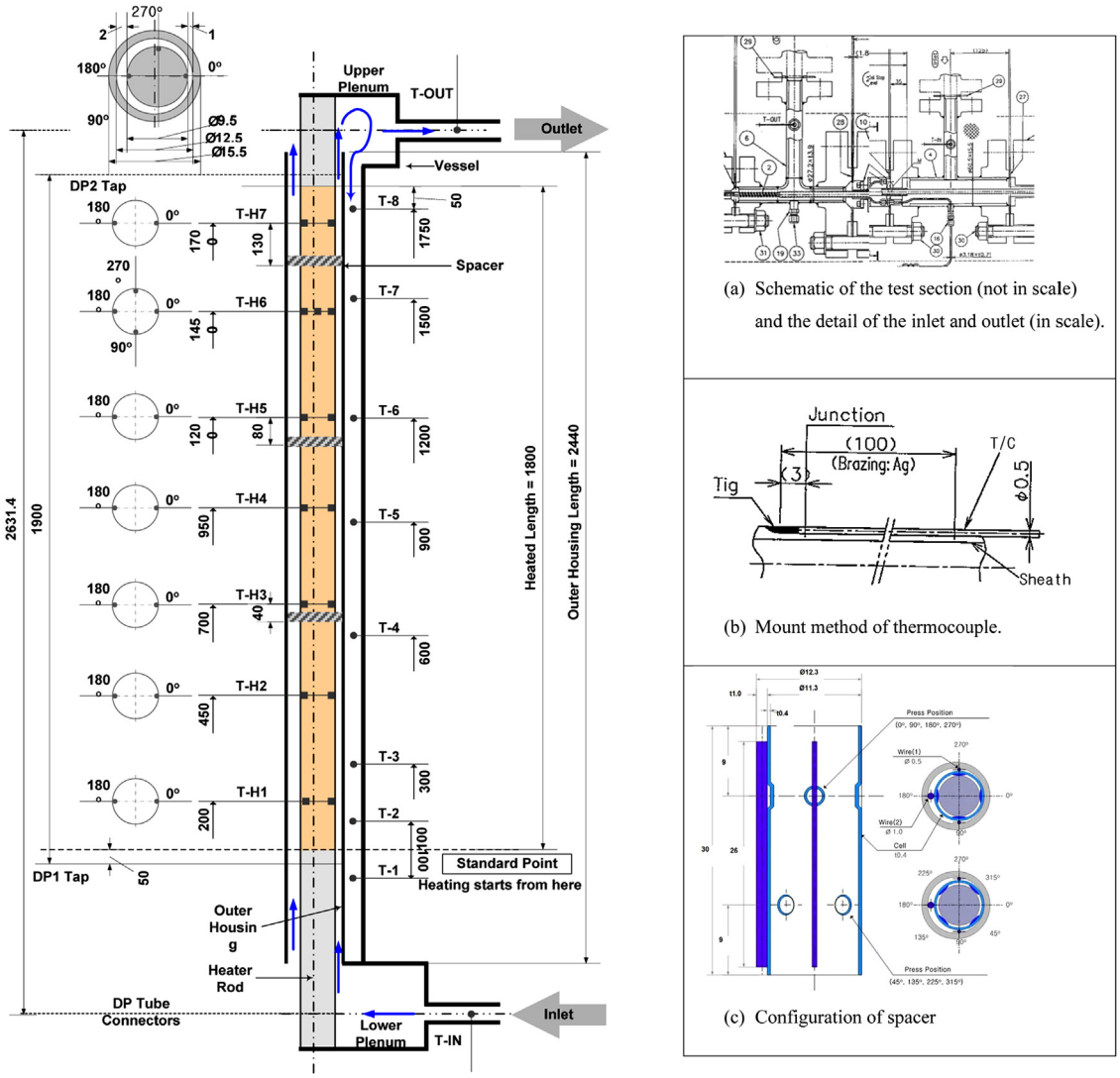

Fig. 4. Test section for eccentric annular channel.

have been an inlet effect. The location of the first row thermocouples were selected as 200 mm downstream from the bottom of the heated section such that the inlet effect was minimized, but it was eventually proved to be insufficient. The numbers in the legend are the inlet fluid temperature measured at the inlet plenum with the orientation of the thermocouple in parenthesis. Zero (0°) and 180° correspond to the narrowest and widest gap of the channel, respectively. The bulk temperature was calculated based on the energy balance neglecting the heat loss with an assumption that fluid enthalpy increases through the addition of electrical heat input. The black solid lines in the figures for the heat transfer coefficient were obtained from a correlation of Dittus–Boelter (1930).

Fig. 5 shows the experimental results for a heat fluxes of 30 and 50 kW/m^2 when the pressure and mass flux were kept constant as 7.75 MPa and 400 kg/m^2 s. The solid symbols correspond to the data measured by the thermocouples along the narrowest gap (0°), and the open symbols correspond to the data obtained from the opposite side (along the widest gap). The wall temperatures in the narrowest gap are consistently higher than those in the widest gap, except for the temperatures measured at the 7th row T/C. When the heat flux was 30 kW/m^2, the wall temperature increased by keeping an almost uniform difference from the bulk temperature. On the contrary, when the heat flux was increased to 50 kW/m^2, the wall temperature considerably increased before the bulk temperature reached the pseudo-critical temperature. This obviously indicates an occurrence of heat transfer deterioration. The maximum temperature difference between the data from the narrowest and widest gap was 4.1 °C for 30 kW/m^2 and 8.2 °C for 50 kW/m^2, respectively. The effect of a spacer was clearly shown by a sudden temperature drop occurring at the 3rd row thermocouples right after the first spacer (10 mm downstream of the first spacer trailing edge corresponding to approximately $3D_h$). Its effect was more evidently shown for 50 kW/m^2. The significant temperature drop may be explained by an argument that the flow field may have become laminar or weakly turbulent owing to the buoyancy and accompanying acceleration caused by a density decrease; and in this circumstance, a slight disturbance will result in a rapid transition of the flow into a turbulent regime. It should be noted that the effect of a spacer did not appear at the 5th and 7th row thermocouples to which the distances from the spacer trailing edges were 50 and 100 mm (corresponding to approximately $17D_h$ and $33D_h$), respectively. Presumably, the disturbed flow field quickly returned to the state corresponding to the local boundary conditions. As the heat flux increased from 30 to 50 kW/m^2, the heat transfer coefficient decreased. This decrease was due to the combined effect of the heat transfer deterioration at high heat flux and property variation. The Dittus–Boelter correlation predicted the experimental

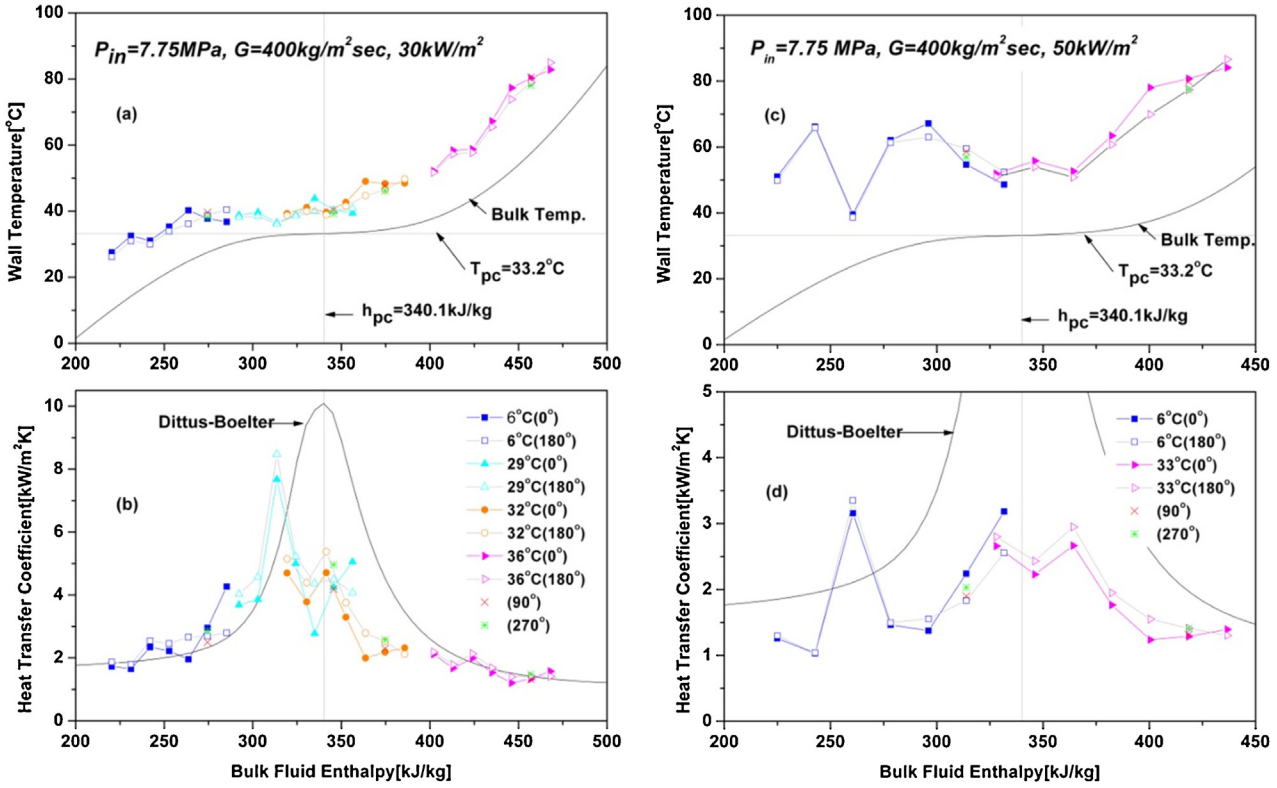

Fig. 5. Distribution of wall temperature along the heater rod surface and calculated heat transfer coefficient: $p = 7.75$ MPa, $G = 400$ kg/m^2 s, $q = 30$, and 50 kW/m^2. (The temperatures in the legend represent the inlet temperature. The degrees represent the orientation shown in Fig. 4(a). This symbols apply to all Figures followed.)

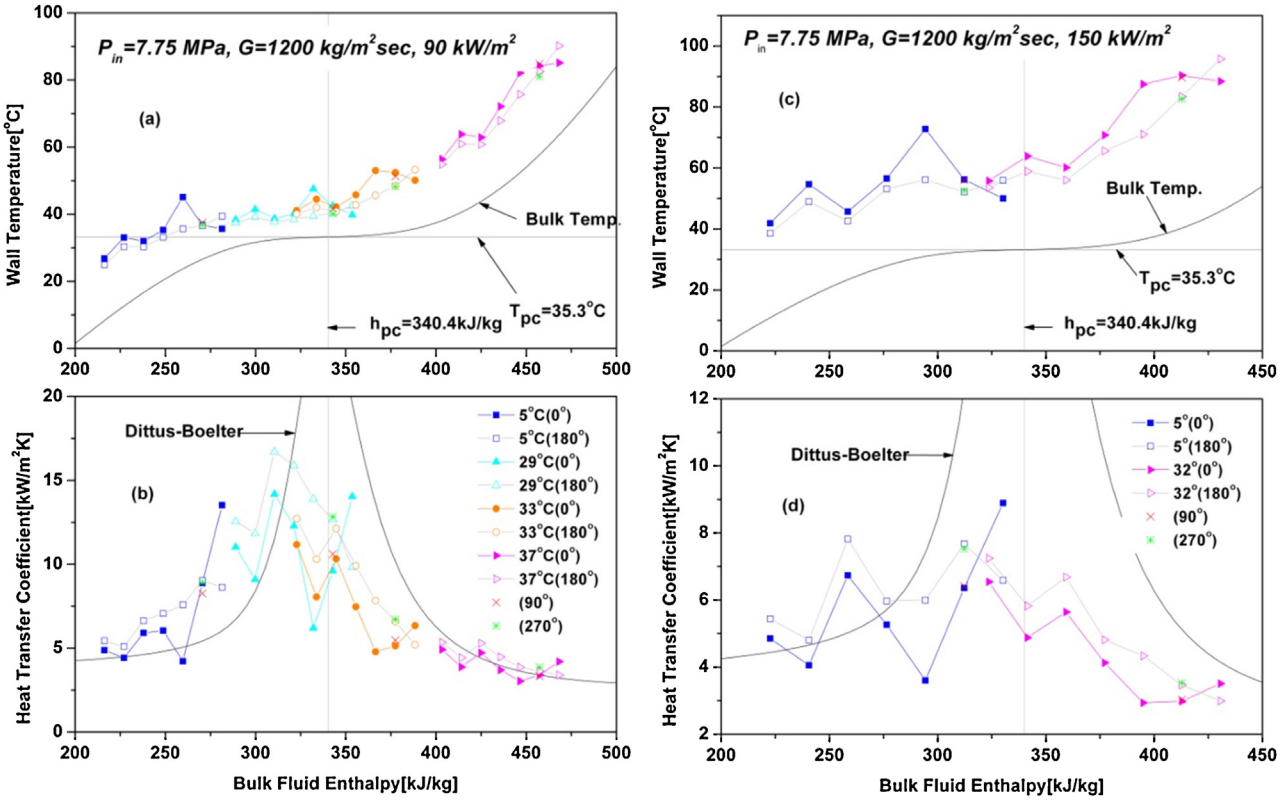

Fig. 6. Distribution of wall temperature along the heater rod surface and calculated heat transfer coefficient: $p = 7.75$ MPa, $G = 1200$ kg/m^2 s, $q = 90$, and 150 kW/m^2.

data for 30 kW/m^2 reasonably well, except for the region around the pseudocritical temperature, while it failed totally for 50 kW/m^2. It should be noted that the 7th row data showed a reversed behavior, where the wall temperatures in the narrowest gap were lower than those at the widest gap. This phenomenon occurred in all cases regardless of the test conditions. This unexpected behavior can be attributed to some kind of defect in the test section or an unexplained flow behavior such as a swirl. Another plausible explanation will be the initiation of an asymmetric flow at around the location of the 6th row thermocouples. The proximity of the row 6 and 7 thermocouples to the outlet nozzle, which was installed perpendicular to the flow channel, may have induced a swirl (possibly asymmetrical too) motion around the heater rod and made the flow speed in the narrower gap higher than that in the wider gap, resulting in low temperatures and higher heat transfer coefficients in the narrow gap. However, the high temperature consistently occurring at 5th row in the narrower side is still to be explained through an experiment with a more sophisticated measuring apparatus or possibly using a numerical simulation.

Fig. 6 shows experimental results similar to those in Fig. 5 for a heat flux of 90 and 150 kW/m^2 keeping the pressure and mass flux constant as 7.75 MPa and 1200 kg/m^2 s. The wall temperature difference between the narrowest and widest gaps was more clearly seen in this case for both heat fluxes. The heat transfer behavior was almost the same as for the case shown in Fig. 5. In this figure the abnormality of the 5th and 7th row thermocouples was evident.

As shown in Fig. 4(a), four (4) thermocouples were installed in the 6th row to see the circumferential temperature distribution. The measured data showed that the temperature at the thermocouple of 90° was close to that of 0°, and the temperature at the thermocouple of 270° was close to that of 180°. However, the differences were so small that it is not discernible in Figs. 5 and 6.

The pressure effect on the supercritical heat transfer was studied by comparing the results for two different pressures. The tested pressures were 7.75 and 8.12 MPa, which are 105 and 110% of the critical pressure, respectively. Fig. 7 shows the wall temperature distributions for the two cases. They were almost identical, and the pressure effect may be concluded as trivial. However, in a test on tubes with three different diameters, the pressure effect (as is in this study, the data was produced for 7.75 and 8.12 MPa) was observed, although the extent of the effect was not very significant. The wall temperatures at a higher pressure were higher than those for a lower pressure (Kang, 2007; Kang et al., 2007). The pressure effect will become significant as the pressure approaches the critical pressure, where the continuity in the physical properties almost breaks (Kang and Chang, 2009). This subject was not included in the present study and is left for a further study.

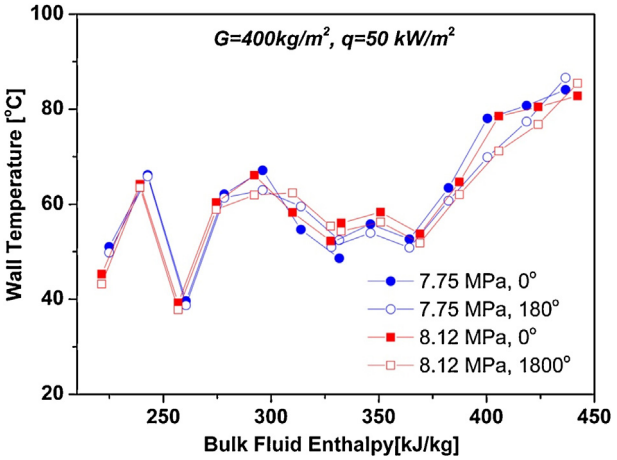

Fig. 7. Wall temperature distribution along both the narrow and wide sides of an eccentric annulus channel at pressures of 7.75 and 8.12 MPa (G = 400 kg/m^2 s, q = 50 kW/m^2).

In Fig. 8 the experimental results for the eccentric and concentric annular channel (designated as 'Ecc' and 'Con', respectively) were compared with each other. The comparison was made to show how different they are from each other; nevertheless the hydraulic diameter of the concentric channel 2 mm is different from that of the eccentric channel 3 mm. The details of the test for a concentric annular channel were reported in earlier papers published by the author's group (Kim et al., 2008; Bae, 2011). The gap size of the concentric annular channel was 1 mm. The overall temperature distributions in the eccentric channel were slightly higher than those of the concentric channel except for the region where the temperature dropped by the spacer effect. In the case of 400 kg/m^2 s and 30 kW/m^2, which seemed to be normal or showed negligible heat transfer deterioration, the temperature distribution in the eccentric channel was almost similar to that in the concentric channel, while they became slightly higher as the bulk temperature exceeded the pseudocritical temperature. However, this trend appeared in the case of 400 kg/m^2 s and 30 kW/m^2, and was not repeated in the case of 400 kg/m^2 s and 50 kW/m^2, where heat

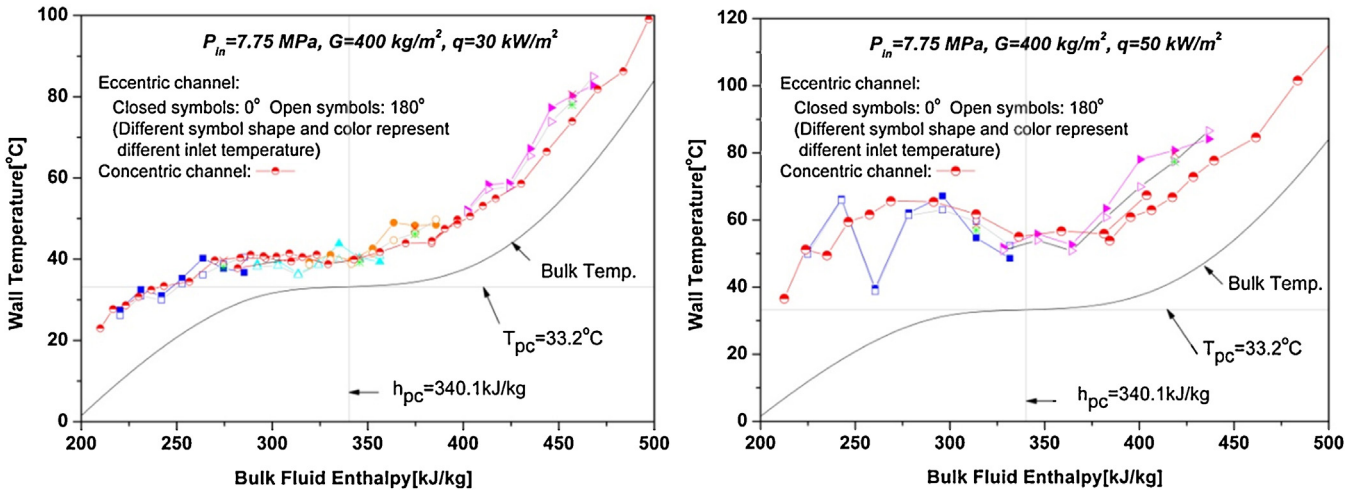

Fig. 8. Comparison of the test results between concentric and eccentric channels at p = 7.75 MPa, G = 400 kg/m^2 s, q = 30 and 50 kW/m^2.

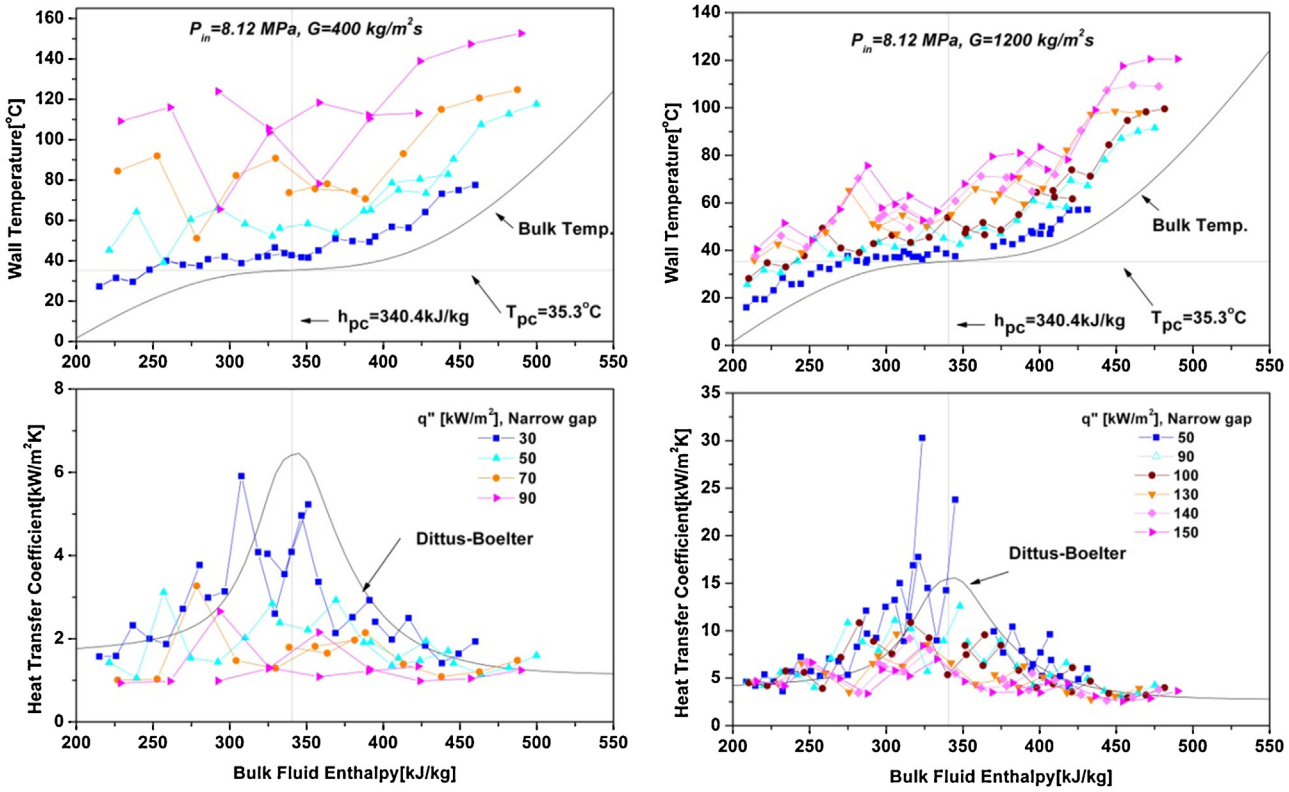

Fig. 9. Effect of heat flux for mass fluxes of 400 and 1200 kg/m^2 s.

transfer deterioration was apparent. In this case, the temperatures in the eccentric channel are higher than those in the concentric channel. Considering that the hydraulic diameters of the concentric and eccentric channel are 2.0 mm and 3.0 mm, respectively, the results shown in Fig. 8 can be regarded as consistent with the results of Bae et al. (2010), where it was reported that a smaller tube diameter resulted in a higher heat transfer coefficient.

In Fig. 9 the effect of heat flux on the wall temperature and heat transfer coefficient was shown for a mass flux of 400 and 1200 kg/m^2 s. Here, the data are provided for a pressure of 8.12 MPa instead of 7.75 MPa for completeness, since the data for 7.75 MPa has been given in the course of the discussions given above. As naturally expected, the wall temperature increased as the heat flux increased. The effect of the mass flux can be easily seen when we compare the plots for the same heat flux shown in the left and right graphs in Fig. 9.

The normalized experimental Nusselt numbers are plotted in Fig. 10 against the non-dimensional buoyancy parameter, which is defined as (Jackson and Hall, 1979)

$$Bu = \frac{\overline{Gr}_b}{Re_b^{2.7}}. \quad (1)$$

The authors suggested that when the value of Bu exceeds 10^{-5}, deterioration of the heat transfer occurs. The correlation used in the normalization is a slightly modified version of the one suggested by Watts and Chou (1982), such as

$$Nu_b = 0.021 Re_b^{0.8} \overline{Pr}_b^{0.55} \left(\frac{\rho_w}{\rho_b}\right)^{0.35}. \quad (2)$$

In addition to Eq. (2) there are many correlations in the literature, however, they are usually valid only for the particular cases where they were derived from, and when applied to other cases,

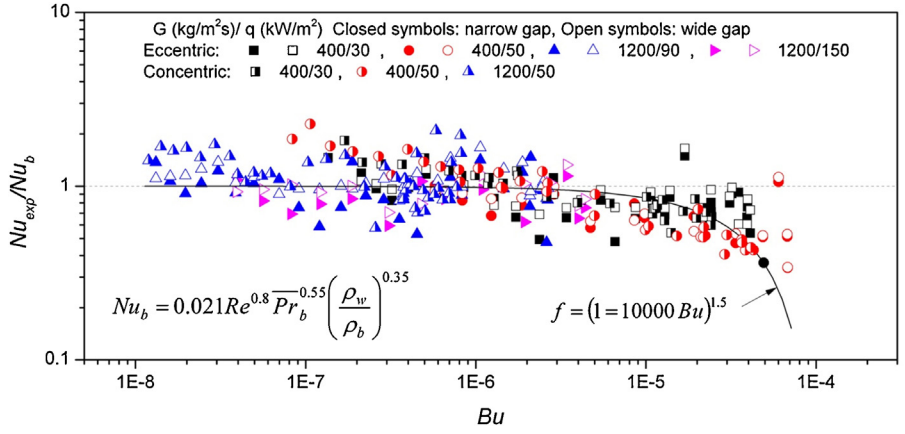

Fig. 10. Normalized experimental Nusselt number as a function of non-dimensional buoyancy parameter.

result in large errors (Bae, 2011). Eq. (2) was selected, as it best represents the data for normal cases in our previous experiments performed at KAERI. The function f in Fig. 10 implies the ratio of the experimental Nusselt number to the value calculated from Eq. (2) (Bae, 2011). In the region of $Bu > 10^{-5}$, deterioration of heat transfer ($f < 1$) was evident. When the mass flux was 400 kg/m^2 s, the heat transfer enhancement was more outstanding than in the cases of 1200 kg/m^2 s. When the value of Bu was smaller than 10^{-6}, the value of function f was close to unity, although there was non-negligible scattering; this probably means that the Nusselt number (or heat transfer coefficient) could be safely calculated from Eq. (2) with a reasonably allowable safety margin. The open symbols are systematically located above the corresponding closed symbols, implying that in the wide side of the channel, the heat transfer occurred more effectively than in the narrow side. The overall thermal performance in the eccentric annular channel was not much different from the concentric counterpart except for the spacer effect.

4. Conclusions

As a continuation of the experiment for a concentric annular channel with a hydraulic diameter of 3 mm, an experiment for an eccentric annular channel was performed. The inner diameter of the outer tube was 12.5 mm. The narrowest gap was 1 mm and the widest was 2 mm. At the same time, the effect of a spacer was investigated by locating three simple spacers upstream of the thermocouples with distances of 10, 50, and 100 mm, respectively. The findings from the experiment are as follows:

- The wall temperature distribution in the narrowest gap was consistently higher than that in the widest gap. A low velocity or weak turbulence (or possible by laminarization) may be responsible for the higher temperature in the narrowest gap.
- The spacer effect was considerable at the 3rd row thermocouples located 10 mm (approximately $3D_h$) downstream of the first spacer (the lowest one), while almost no effect was observed at the 5th and 7th row thermocouples located $17D_h$ and $33D_h$ downstream of the 2nd and 3rd spacers, respectively. The flow at the location of the 5th and 7th row thermocouples may well have returned to the state corresponding to the local boundary conditions.
- The pressure effect was marginal in the case studied in this paper. However, the pressure effect will become stronger as the pressure approaches the critical pressure, where the continuity in the physical properties almost breaks. This is left for further investigation.
- The overall temperature distributions in the eccentric channel were slightly higher than in the concentric case except for the region affected by the spacers. This is consistent with the results previously obtained in the test for tubes. The difference may be attributed to the difference in the hydraulic diameter. However, the overall thermal behavior was not much different from that in the concentric counterpart.

It should be admitted that an eccentric annular channel definitely has a limitation in representing the subchannels in a fuel assembly for a proposed design by KAERI. First, it cannot exactly simulate the interactions between subchannels. Secondly, the surrogate medium CO_2 has an inherent scaling problem, which is one of the issues to be resolved. The interpretation of the results for CO_2 into those for water is not straightforward either. However, the results obtained in this work will certainly provide useful first-hand information, although qualitative, for the development of an SCWR.

Acknowledgments

The author would like to acknowledge the financial support by the Nuclear Research & Development Program of the National Research Foundation of Korea (NRF) grant funded by the Korean Government (MSIP). (Grant code: NRF-2012M2A8A2025682). Without the exceptional effort exerted by Mr. Kang Deog-Ji, who had excellently performed the whole experiment as well as data processing, this paper could not have been written. Dr. Kim Hwan-Yeol has also provided invaluable comments and suggestions during the experiment and subsequent analysis.

References

Bae, Y.Y., Jang, J.S., Kim, H.Y., Yoon, H.Y., Kang, H.O., Bae, K.M., 2007. Research activities on a supercritical pressure water reactor in Korea. Nucl. Eng. Technol. 39 (4), 273–286.

Bae, Y.Y., Kim, H.Y., 2008. Convective heat transfer to CO_2 at a supercritical pressure flowing vertically upward in tubes and an annulus channel. In: 16th International Conference on Nuclear Engineering, Orlando, FL, USA, May 11–15.

Bae, Y.Y., Kim, H.Y., Kang, D.J., 2010. Forced and mixed convection heat transfer to supercritical CO_2 vertically flowing in a uniformly-heated circular tube. Exp. Therm. Fluid Sci. 34, 1295–1308.

Bae, Y.Y., 2011. Mixed convection heat transfer to carbon dioxide flowing upward and downward in a vertical tube and an annular channel. Nucl. Eng. Des. 241, 3164–3177.

Dittus, F.W., Boelter, L.M.K., 1930. University of California, Publications of Engineering, vol. 2., pp. 443.

Jackson, J.D., Hall, W.B., 1979. Influences of buoyancy on heat transfer to fluids flowing in vertical tubes under turbulent condition. In: Kakac, S., Spalding, D.B. (Eds.), Turbulent Forced Convection in Channels and Bundles. Hemisphere Publishing, Washington, New York, London, pp. 613–640.

Jackson, J.D., 2002. Consideration of the heat transfer properties of supercritical pressure water in connection with the cooling of advanced nuclear reactors. In: 13th Pacific Basin Nuclear Conference, Shenzhen City, China, October 21–25.

Kang, D.G., 2007. Heat Transfer Characteristics for an upward Flowing Supercritical Pressure CO_2 in a Vertical Circular Tube. Cheju University (in Korean, MS Thesis).

Kang, D.G., Kim, S., Bae, Y.Y., Kim, H.Y., Kim, H., 2007. Effect of tube diameter on heat transfer to vertically upward flowing supercritical CO_2. In: Transactions of Korean Nuclear Scarcity Spring Meeting, Jeju, Korea, May 10–11.

Kang, K.H., Chang, S.H., 2009. Experimental study on the heat transfer characteristics during the pressure transients under supercritical pressures. Int. J. Heat Mass Transfer 52, 4946–4955.

Kim, H., Kim, H.Y., Song, J.H., Bae, Y.Y., 2008. Heat transfer to supercritical pressure carbon dioxide flowing upward through tubes and a narrow annulus passage. Prog. Nucl. Energy 50, 518–525.

Komita, H., Morooka, S., Yoshida, S., Mori, H., 2003. Study on the heat transfer to the supercritical pressure fluid for supercritical water cooled power reactor development. NURETH-10, Seoul, Korea.

Lemmon, E.W., Huber, M.L., McLinden, M.O., 2010. Reference Fluid Thermodynamics and Transport Properties, NIST Standard Reference Database 23, Version 9.0.

Nouri, J.M., Umur, H., Whitelaw, H., 1993. Flow of Newtonian and non-Newtonian fluids in concentric and eccentric annuli. J. Fluid Mech. 253, 617–641.

Okumura, T., Merzari, E., Ninokata, H., 2006. Direct numerical simulation of turbulent flows in an eccectric annulus channel. ANS Trans. 95, 825–826.

Rapley, C.W., Gosman, A.D., 1986. The prediction of fully developed axial turbulent flow in rod bundles. Nucl. Eng. Des. 97, 311–325.

Sharabi, M., Ambrosini, W., He, S., Jackson, J.D., 2008. Prediction of turbulent convective heat transfer to a fluid as supercritical pressure in square and triangular channels. Ann. Nucl. Energy 35, 993–1005.

Watts, M.J., Chou, C.T., 1982. Mixed convection heat transfer to supercritical pressure water. In: Int. Heat Transfer Conf. München, vol. 3, pp. 495–500.

Waata, C., Schulenberg, T., Cheng, X., Laurien, E., 2005. Coupling of MCNP with a subchannel code for analysis of a HPLWR fuel assembly. In: NURETH-11, Avignon, France.